ACS APPLIED MATERIALS & INTERFACES

www.acsami.org

Research Article

Blue-Emitting $Cs(Pb,Cd)Br_3$ Nanocrystals Resistant to Electric Field-Induced Ion Segregation

Sergey S. Anoshkin,[#] Elizaveta V. Sapozhnikova,[#] Yibo Feng, Yangyang Ju,[*] Alexander Pavlov, Roman G. Polozkov, Alexey Yulin, Haizheng Zhong, and Anatoly P. Pushkarev[*]

Cite This: *ACS Appl. Mater. Interfaces* 2024, 16, 11656–11664

Read Online

ACCESS | Metrics & More | Article Recommendations | Supporting Information

ABSTRACT: High-performance solution-processed perovskite light-emitting diodes (PeLEDs) have emerged as a good alternative to the well-established technology of epitaxially grown $A^{III}B^{V}$ semiconductor alloys. Colloidal cesium lead halide perovskite nanocrystals ($CsPbX_3$ NCs) exhibit room-temperature excitonic emission that can be spectrally tuned across the entire visible range by varying the content of different halogens at the X-site. Therefore, they present a promising platform for full color display manufacturing. Engineering of highly efficient PeLEDs based on bromide and iodide perovskite NCs emitting green and red light, respectively, does not face major challenges except low operational stability of the devices. Meanwhile, mixed-halide counterparts demonstrating blue luminescence suffer from the electric field-induced phase separation (ion segregation) phenomenon described by the rearrangement (demixing) of mobile halide ions in the crystal lattice. This phenomenon results in an undesirable temporal redshift of the electroluminescence spectrum. However, to realize spectral tuning and, at the same time, address the issue of ion segregation less mobile Cd^{2+} ion could be introduced in the lattice at Pb^{2+}-site that leads to the band gap opening. Herein, we report an original synthesis of $CsPb_{0.88}Cd_{0.12}Br_3$ perovskite NCs and study their structural and optical properties, in particular electroluminescence. Multilayer PeLEDs based on the obtained NCs exhibit single-peak emission centered at 485 nm along with no noticeable change in the spectral line shape for 30 min which is a significant improvement of the device performance.

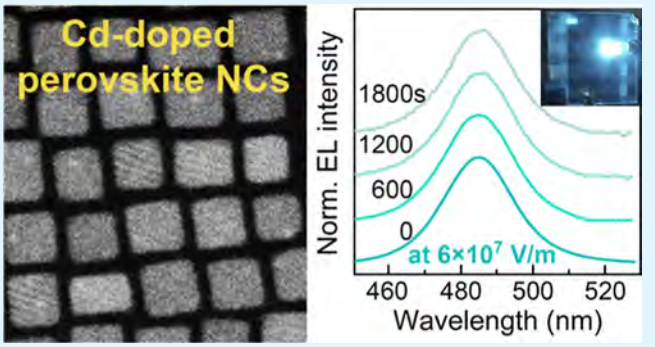

KEYWORDS: *halide perovskite, colloidal nanocrystals, cadmium doping, ion segregation, light-emitting diode*

INTRODUCTION

Over the last eight years, halide perovskite nanocrystals (NCs) have emerged as brightly luminescent materials with tunable band gap for advanced photonics and optoelectronics.[1] Owing to the electronic structure of halide perovskites which defines their "defect tolerance"[2] (i.e., formation of shallow defect states only near the valence band maximum and conduction band minimum), passivation of surface traps using organic ligands[3−6] and relatively large exciton binding energies[7] colloidal solutions of NCs exhibit narrow-band emission with near-unity photoluminescence quantum yield (PLQY) at room temperature. These properties along with large light absorption coefficient[8] and high charge carrier mobility in perovskites[9] promote NCs for the fabrication of high-performance perovskite light-emitting diodes (PeLEDs). Green and red perovskite PeLEDs based on $CsPbBr_3$[10−12] and $CsPbI_3$[3,13,14] NCs, respectively, have recently displayed excellent electroluminescence external quantum efficiencies (EQE) as high as 25%. As compared to homohalide compositions, heterohalide (or mixed-halide) $CsPb(Cl,Br)_3$ perovskites emitting blue light suffer from electric field-driven ion segregation (see Supporting Information in refs 15 and 16) revealing itself in a temporal red-shift of electroluminescence spectrum in biased devices.

Ion segregation in mixed-halide perovskites was initially discovered and further vastly investigated for organo-inorganic $MAPb(Br,I)_3$ (MA—methylammonium) ones. Hoke et al.[17] reported structural and optical evidence of the light-induced formation of Br-rich and I-rich perovskite domains. The latter have a narrower band gap than the former and the initial mixed-halide composition do and therefore act as energy funnels for excited charge carriers or excitons. As a result, a noticeable redshift of photoluminescence (PL) spectrum is observed. The major mechanism of this phenomenon is the migration of mobile halide ions (or their vacancies)[18,19] that could be influenced by forces arising due to the following

Received: December 4, 2023
Revised: February 7, 2024
Accepted: February 9, 2024
Published: February 26, 2024

reasons: (i) sufficient lattice strain occurring at spontaneously formed the heaviest halogen-rich (e.g., I for $MAPb(Br,I)_3$) sites where a photogenerated polaron resides;[20,21] (ii) nonhomogeneous carrier generation rate profile through the thickness of a perovskite film that results in a directional drift of halide ions having different mobility;[22] (iii) minimizing the energy of photoexcited holes when they occupy the heaviest halogen-rich domain showing a low energy valence band edge.[23] In accordance with that, to mitigate halide segregation the approaches aimed at reduction of the number of halide vacancies, minimization of electron−phonon coupling via substituting Cs^+ for polar MA^+ cation, homogeneous mixing of halide ions over the entire volume of perovskite, as well as uniform distribution of the light in this volume were suggested.[21−24]

In the meantime, there is another strategy for composition-dependent spectral tuning in all-inorganic bromide perovskites that affords NCs exhibiting persistent blue emission. Doping of $CsPbBr_3$ NCs with Cd^{2+} ions substituting for Pb^{2+} ones in the crystal lattice has been demonstrated to give $CsPb_{1-x}Cd_xBr_3$ counterparts possessing a direct band gap for x not exceeding 0.25[25] and showing a blueshift of PL peak in the 460−515 nm range with increase in cadmium content.[25−27] Obviously, the ion segregation (i.e., demixing of Cd^{2+} and Pb^{2+}) is suppressed in these materials because both cations are heavy, have a large coordination number of 6, and, hence, are less mobile than light halide ions. Nevertheless, slow Cd diffusion, most likely mediated by doubly negatively charged vacancies (V_{Pb}^{2-} and V_{Cd}^{2-}), and its release from the NCs defective surface into colloidal solution could affect the long-term spectral stability of PL.[25]

In this work, we propose a novel approach to the synthesis of $CsPb_{0.88}Cd_{0.12}Br_3$ NCs showing that blue emission peaked at 485 nm. First, $CsPbBr_3$ NCs are obtained by the hot-injection method and purified from byproducts. Then, their colloidal solution reacts with cadmium oleate and oleylammonium bromide additives to give Cd-doped NCs having a mean size of 11 nm. Furthermore, our approach gives us direct control over Cd doping process dynamics easily derived from the time-dependent PL blueshift of NCs in the reaction mixture. Thus, following a new protocol one can obtain a certain product exhibiting desirable optical properties or a set of required products instead of a single composition of NCs specified by the exact stoichiometric ratio of metal halide salts taken for the conventional hot-injection synthesis. Importantly, the proposed two-step synthesis affords complete mixing of metal(II) cations in the perovskite crystal lattice due to diffusion-assisted slow substitution of Cd^{2+} for Pb^{2+} at 150 °C along with passivation of the NCs surface defect sites by oleylammonium bromide species. Accurate values of the band gap energy for the bulk forms of initial $CsPbBr_3$ and resultant $CsPb_{0.88}Cd_{0.12}Br_3$ perovskites are predicted via density function theory (DFT) calculations. The structure, crystallinity, and chemical content of the Cd-doped NCs are determined using powder X-ray diffraction (XRD), high-resolution scanning transmission electronic microscopy (HRSTEM), and quantitative energy-dispersive X-ray (EDX) spectroscopy methods, respectively. The colloidal solution demonstrates PLQY = 89.9% along with no change in PL line shape for at least 2 months. This is consistent with the experimentally established even distribution of Cd^{2+} in the perovskite crystal lattice and confirms a low concentration of surface defects in NCs. Electroluminescent (EL) properties of NCs are studied on multilayer devices that reveal no noticeable spectral shift at 6×10^7 V m^{-1} for 30 min.

RESULTS AND DISCUSSION

Synthesis of Cs(Pb,Cd)Br_3 NCs. To obtain perovskite NCs doped with Cd^{2+} ions, we employ a novel synthetic approach. First, we prepare a stock solution for the doping procedure by mixing 0.5 mmol of cadmium bromide hydrate ($CdBr_2 \cdot [H_2O]_4$) with 1.2 mmol of oleic acid (OA) and 1.2 mmol of oleylamine (OLAM) in 10 mL of 1-octadecene (ODE) solvent. The mixture reacts under N_2 gas at 150 °C to give a clear solution (for details, see Methods) that is cooled to room temperature and utilized further for the modification of the $CsPbBr_3$ NCs structure. The resultant stock solution contains cadmium oleate $Cd(OA)_2$ and oleylammonium bromide [$Br^- \cdots HOLAm^+$] species that is confirmed by the presence of two peaks at 1640 and 1545 cm^{-1} assigned to protonated amine groups ($-NH_3^+$) and oleate anions ($-COO^-$),[28] respectively, in Fourier-transform infrared (FTIR) spectrum of the solution (Figure S1). Second, a colloidal solution of $CsPbBr_3$ NCs of 11−12 nm size is prepared according to a protocol reported by Protesescu et al.[7] For this, 0.18 mmol of lead bromide ($PbBr_2$) is mixed with 1.58 mmol of OA and 1.52 mmol of OLAm in 5 mL of ODE at 120 °C. The mixture is stirred and heated up to 180 °C under N_2 gas to give a clear perovskite precursor solution. As the temperature reaches 180°, 0.05 mmol of preliminary prepared cesium oleate (CsOA) in the ODE (for details, see Methods) is quickly injected into the precursor solution. After injection, colloidal $CsPbBr_3$ NCs form immediately. We let this colloidal solution react for 10 s and, thereafter, quench the reaction using an ice bath. The colloidal solution is diluted with 15 mL of ODE and centrifuged at 5000 rpm for 5 min. Then, we discard a supernatant solution, redisperse the obtained sediment in 15 mL of ODE, and add to it 0.018 mmol of $Cd(OA)_2$ and 0.036 mmol of [$Br^- \cdots HOLAm^+$] species (0.320 g of the stock solution). Such an addition causes an immediate rise in PL of the colloidal solution (see the image with two vials in Figure 1), obviously, because of the passivation of the crystal lattice defects at the NCs surface. The resultant mixture undergoes vacuumization and then is stirred under N_2 gas at 150 °C for 1 h. A schematic illustration of the synthesis is presented in Figure 1. We trace the dynamics of the doping process by blueshift of the PL maximum of the aliquots taken during the reaction (central bottom image in Figure 1). Since the reaction occurs at a limited concentration of $Cd(OA)_2$, it reveals exponential dynamics that is confirmed by the time-dependent blueshift described by the function $\lambda_{max}(t) = \alpha \exp\left(-\frac{t}{\tau}\right) + \beta$, where α = 20 nm, β = 485 nm, and τ = 13 min that give the value $\lambda_{max}(0)$ = 505 nm corresponding to the first aliquot taken right at the moment when the temperature reaches 150 °C. As a result, we obtain 485 nm blue-emitting Cs(Pb,Cd)Br_3 NCs for 1 h (Figure 1). The final product is sedimented by centrifugation at 5000 rpm for 5 min and redispersed in 20 mL of *n*-hexane.

Modeling. We assume the stirring of $CsPbBr_3$ NCs with the additive at 150 °C results in the reaction of $Cd(OA)_2$ with perovskite NCs. In this reaction, Cd^{2+} ions substitute for Pb^{2+} ones at the surface and then the former undergo inward diffusion while the latter diffuse toward the surface where they tend to be released in the form of $Pb(AO)_2$. Meanwhile, [$Br^- \cdots HOLAm^+$] species passivate surface vacancies at halogen- and

https://doi.org/10.1021/acsami.3c18122
ACS Appl. Mater. Interfaces 2024, 16, 11656−11664

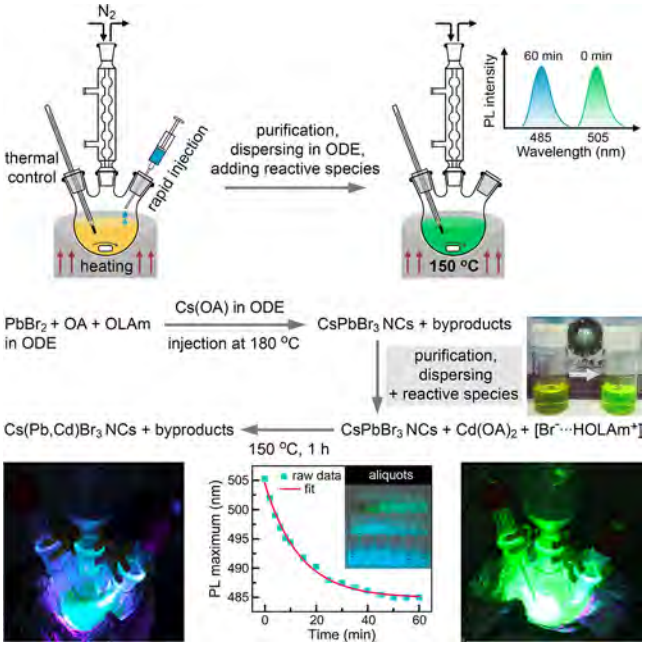

Figure 1. Schematic illustration of the synthesis of Cd-doped colloidal perovskite NCs. After the preparation of $CsPbBr_3$ NCs, they are purified and mixed with the reactive species for doping. Adding the reactive species causes an immediate increase in PL of the colloidal solution as shown in the image with two vials. When the mixture is stirred at 150 °C under N_2 gas, Cd^{2+} ions substitute for Pb^{2+} ones in the perovskite crystal lattice which results in a gradual blueshift of PL spectrum of NCs. The bottom images show the color of PL before (right picture) and at the end (left picture) of the doping procedure. The time-dependent blueshift of the PL maximum is presented in a central bottom plot. Inset image demonstrates the gamut of PL for the series of aliquots taken during the reaction: in every row of aliquots Cd content in NCs increases from left to right and reaches the maximum value for the right sample in the front row. Note the samples on the left side look brighter because UV light excites the entire set from the left as well.

cesium-site and, thus, preserve bright PL (Figure 2a). According to quantitative EDX analysis (see Structural and Optical Properties subsection), the resultant product of our synthesis exhibiting emission centered at 485 nm contains approximately 12% of Cd^{2+}. This is consistent with data reported by Imran et al.[25] Taking this into account, we conduct theoretical modeling of the crystal structures of initial and resultant perovskites as well as estimate band gap energies for them to verify remarkable differences in PL.

The DFT calculations are performed to determine the crystal structure and band structure for orthorhombic $CsPbBr_3$ and $CsPb_{0.875}Cd_{0.125}Br_3$ perovskites (for details, see Methods). The latter one can be easily generated by substitution of 1/8 of Pb atoms with Cd atoms in 2 × 2 × 1 translation of the $CsPbBr_3$ unit cell. This makes calculations much less time-consuming than in the case of $CsPb_{0.88}Cd_{0.12}Br_3$. Meanwhile, we believe that such a small alteration of the composition does not change the band gap value of the studied Cd-doped perovskite significantly. As expected, the crystal lattice for the latter is more compact as compared to that of the former: a = 7.97 Å, b = 8.29 Å, c = 11.56 Å for $CsPb_{0.875}Cd_{0.125}Br_3$, and a = 7.91 Å, b = 8.43 Å, c = 11.67 Å for $CsPbBr_3$. The structures are presented in Figure 2b. It is known that the band gap values close to experimentally measured for $CsPbBr_3$ can be obtained from DFT calculations using conventional Perdew–Burke–Ernzerhof (PBE)[29] exchange-correlation potential[30] without spin–orbit coupling (SOC). This happens because generalized gradient approximation level calculations often underestimate the band gap values of materials[31−33] and the SOC effect can significantly lower the calculated band gap values of Pb-based halide perovskites.[34,35] In the case when Cd atoms substitute for Pb ones, the effect of SOC on the band structure of material can change drastically and, thus, a more accurate calculation procedure which incorporates SOC needs to be employed. The calculation procedure described in the Methods section provides the accurate band gap value (2.34 eV) for $CsPbBr_3$[36] with an account of SOC, no free parameters, and a fraction of the cost of more advanced *meta*-GGA or hybrid exchange-correlation potentials. Introducing 12.5% of cadmium in the crystal lattice instead of lead gives the opening of the band gap from 2.34 up to 2.49 eV depicted in the corresponding k-dependent spectral function plots in Figure 2b. For $CsPbBr_3$, the value is very close to experimentally derived 2.31 eV for bulk perovskite.[37] On this basis, we believe 2.49 eV is also a quite accurate value for bulk $CsPb_{0.875}Cd_{0.125}Br_3$.

Structural and Optical Properties. To evaluate the impact of Cd-doping on structural transformations, powder XRD of NCs thick film deposited on a glass substrate is conducted. In comparison with the reference data for orthorhombic $CsPbBr_3$ (space group *Pbnm*),[38] the obtained $Cs(Pb,Cd)Br_3$ NCs demonstrate a small shift of the diffraction peaks to larger 2θ angles, in particular a peak at ca. 30° undergoes 0.2° shift (Figure 3a). At the same time, it is established that all the diffraction peaks in the pattern of purified as-prepared $CsPbBr_3$ NCs match perfectly with the reference ones (Figure S2). On the basis of XRD data, the angle difference between centers of (110) diffraction peaks of $CsPbBr_3$ and Cd-doped NCs is 0.08° 2θ only. This implies that Cd doping in our synthesis causes a lattice contraction of 0.5% in the [110] crystallographic direction. Indeed, the replacement of Pb^{2+} with Cd^{2+} possessing a smaller ionic radius than the former results in a decrease in the volume of the crystal unit cell and, therefore, makes the crystal lattice slightly more compact. A similar trend was observed by Imran et al.[25] (see Supporting Information). A mean size for NCs is estimated from low-magnification scanning transmission electron microscopy (STEM) images and equals 11 nm (Figure 3b). HRSTEM image (Figure 3c) and fast Fourier transform (FFT, Figure 3d) of the captured NC reveal its excellent crystallinity and the distance of 0.58 nm between the (002) crystallographic planes. It is worth noting that we do not observe any Pb/Cd–Br sublattice[25] in the high-resolution image because of an even distribution of Cs, Pb, Cd, and Br atoms in NCs confirmed by EDX mapping analysis of a triad (Figure 3e). For the determination of the exact chemical content of the NCs, a concentrated colloidal solution is drop-casted on the surface of a silicon substrate that is further sealed in a 10 mL centrifuge tube to let the solvent slowly evaporate. This procedure gives a thick film along with perovskite superlattices[39] (Figures 3f and S3) that are measured by quantitative EDX spectroscopy. The EDX spectrum demonstrates major signals for Br, Pb, and Cs atoms, as well as a minor one for Cd (Figure 3g). According to the spectrum, our NCs have a composition close to $CsPb_{0.88}Cd_{0.12}Br_3$.

Owing to the incorporation of Cd^{2+} instead of Pb^{2+} into perovskite lattice the absorption and PL spectra shift to the blue region by 28 nm as compared to those of initial $CsPbBr_3$

https://doi.org/10.1021/acsami.3c18122
ACS Appl. Mater. Interfaces 2024, 16, 11656−11664

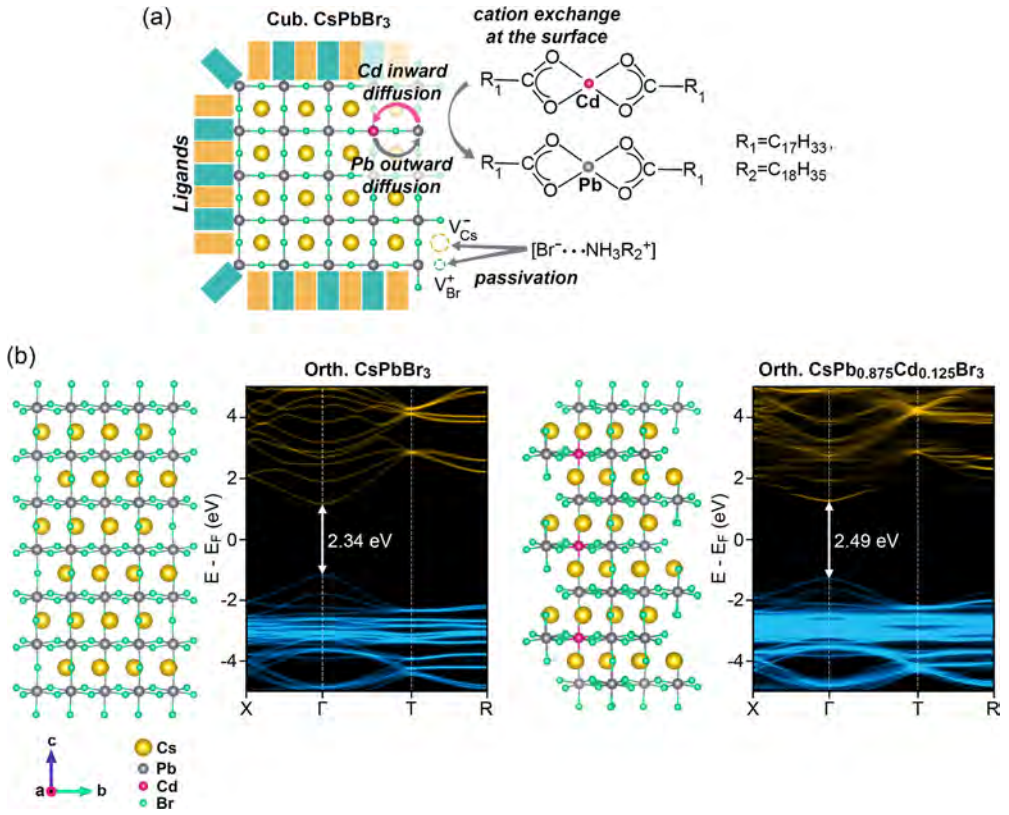

Figure 2. (a) Schematic illustration of the formation of mixed-cation perovskite structure along with passivation of defect states to preserve highly efficient luminescence. For this, the cubic $CsPbBr_3$ structure has been chosen because the formation occurs at 150 °C temperature. Cd oleate molecule reacts with the Pb ion at the surface to give the Pb oleate counterpart and surface Cd ion that further diffuses inward the NC. [Br^-···$HOLAm^+$] species passivate Br^--site (V_{Br}^+) and Cs^+-site (V_{Cs}^-) vacancies at the surface. (b) Calculated crystal structures of orthorhombic $CsPbBr_3$ and $CsPb_{0.875}Cd_{0.125}Br_3$ and corresponding energy band diagrams for them. The color intensity is proportional to the density of states. The bands were unfolded with respect to the optimized $CsPbBr_3$ structure.

NCs (Figure S4). The colloidal solution exhibits a single peak centered at 485 nm with a full width at half-maximum of 19.5 nm (Figure 3h). The latter value is 2 nm larger than that of nondoped counterpart. Such a shift and broadening of the PL spectrum is explained by the phenomenon of the opening of a band gap as follows: the larger the Cd content in the lattice, the less dispersive the conduction band minimum at the Γ point and the closer its energy to the vacuum level along with the stronger the stabilization of the band at the *R*-point emerging from the bonding orbital overlap of the empty 5s orbitals of Cd with the unoccupied 6p of Pb.[25] Furthermore, we emphasize that the colloidal solution of our NCs shows almost 90% PLQY and exhibits spectrally stable emission for 2 months (Figure 3i). These data demonstrate significant improvement in comparison with PLQY = 82% for previously reported $CsPb_{0.88}Cd_{0.12}Br_3$ NCs that suffer from structural instability related to the release of Cd species and, therefore, experience pronounced redshift of PL spectrum for 14 days.[25] We assume the established improvement of optical properties stems from our synthetic approach that affords Cd^{2+} ions to slowly substitute for Pb^{2+} ones at the surface of NCs and diffuse inward at 150 °C resulting in their even distribution in the crystal lattice proven by EDX mapping (Figure 3e). In addition, [Br^-···$HOLAm^+$] species in the reaction could act as a source of Br^- ions preventing the generation of positively charged halide vacancies and $HOLAm^+$ ions passivating negatively charged vacancies at the surface. Thus, the successful healing of surface defects effectively suppresses the release of Cd species in the solution as well as reduces nonradiative exciton recombination.

Perovskite NCs-Based LEDs. EL properties of Cd-doped NCs were examined on multilayer devices possessing an architecture similar to one reported by Vashishtha et al. (see Supporting Information in ref 40). The device configuration consists of consequently spin-casted on top of indium tin oxide (ITO) anode hole injection poly(3,4-ethylenedioxythiophene) poly(styrenesulfonate) (PEDOT/PSS), hole-transporting poly(4-butylphenyl-diphenyl-amine) (polyTPD), electron-blocking polyvinylcarbazole (PVK), and emissive NCs layers that are covered with electron-transporting 1,3,5-tris(1-phenyl-1*H*-benzimidazol-2-yl)benzene (TPBi) layer and LiF/Al cathode deposited by thermal evaporation in a vacuum chamber (Figure 4a, for details, see Methods). In such a device, electrons are injected from the lowest unoccupied molecular orbital of TPBi into the conduction band of the NCs, while holes are transferred from the highest occupied molecular orbital of PVK into the valence band. Furthermore, a thin PVK layer prevents the leakage of electrons from the active layer and their undesirable recombination with holes in polyTPD. To balance concentrations of the injected electrons and holes in the emissive layer for their efficient radiative recombination we vary the thickness of layers. It is established that ITO/PEDOT/PSS (40 nm)/polyTPD (20 nm)/PVK (5 nm)/$CsPb_{0.88}Cd_{0.12}Br_3$ NCs (15 nm)/TPBi (20 nm)/LiF (1 nm)/Al (120 nm) structure demonstrates the highest performance: turn-on bias of 4.5 V, maximum brightness of 138.7 cd

https://doi.org/10.1021/acsami.3c18122
ACS Appl. Mater. Interfaces 2024, 16, 11656−11664

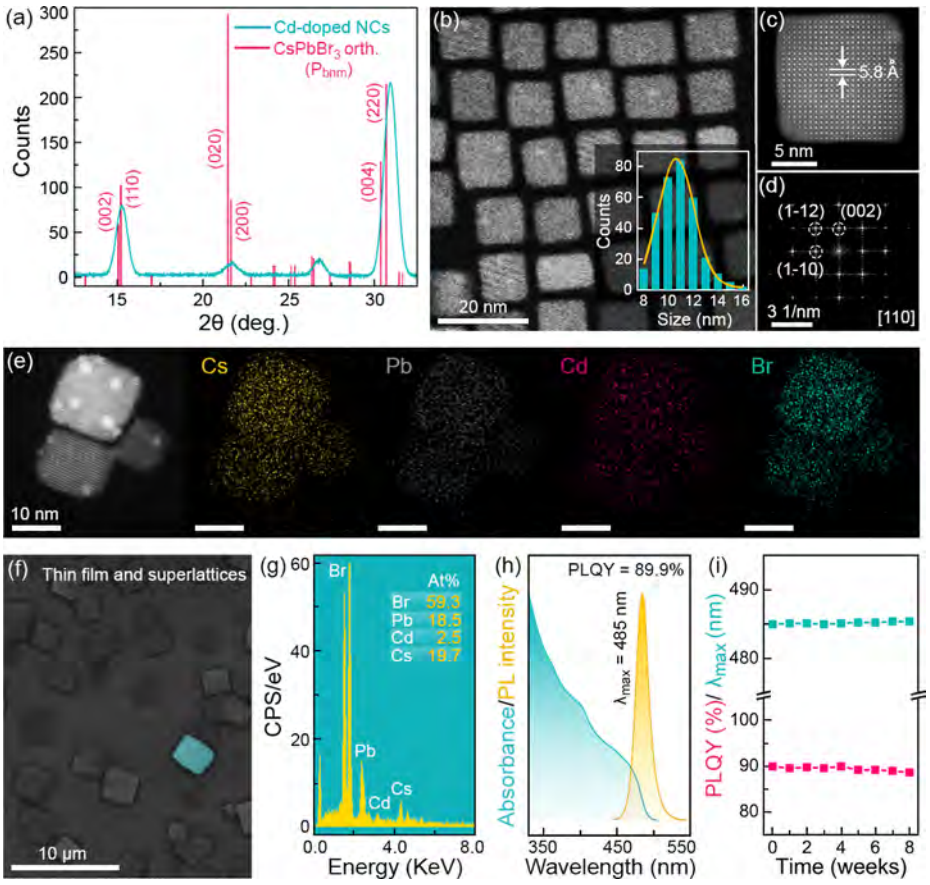

Figure 3. (a) XRD pattern for $Cs(Pb,Cd)Br_3$ NCs and the reference data for orthorhombic $CsPbBr_3$ perovskite (space group *Pbnm*). (b) Low-magnification STEM image of an ensemble of NCs. Inset plot shows a histogram of the size distribution of NCs and Gaussian fit giving a mean size of 11 nm. (c) HRSTEM image of an isolated NC demonstrating 0.58 nm distance between (002) crystallographic planes. (d) FFT image of the NC measured along the [110] zone axis and confirming its high crystallinity because of the observation of sharp and bright spots, in particular corresponding to (002), (1−10), and (1−12) planes. (e) EDX mapping of an NCs triad showing an even spatial distribution of Cs, Pb, Cd, and Br atoms in the perovskite crystal lattice. (f) SEM image of NCs deposited on a silicon substrate in the form of thin film and microscopic superlattices. (g) EDX spectrum of a single superlattice (the stained one in the SEM image) revealing a chemical content of NCs close to $CsPb_{0.88}Cd_{0.12}Br_3$. (h) Absorption and PL spectra of diluted colloidal solution of the NCs. (i) 8 weeks dynamics of PLQY and wavelength of PL peak maximum for NCs colloidal solution in *n*-hexane.

m^{-2} at 8.5 V (Figure 4b), and maximum EQE = 0.038% at current density of 69.25 mA cm^{-2} (Figure 4c). This device performance is much higher than that of one based on blue-emissive mixed-halide $CsPbCl_{1.5}Br_{1.5}$ NCs[15] (pink curve in Figure 4c).

The fabricated devices show sky-blue electroluminescence (see the inset image in Figure 4b) which is identified by (*x* 0.13; *y* 0.25) coordinates in the CIE 1931 color diagram (Figure 4d). The single-peak emission is centered at 485 nm and does not undergo any spectral shift with an increase in applied bias up to 8.5 V (Figure 4d) that is not true for single-layer devices based on mixed-halide Cl−Br perovskites revealing a new peak with a longer wavelength when bias exceeds 4 V.[41] Finally, we test the temporal stability of the EL spectrum at a bias of 6 V. Taking into account the overall thickness of the sandwich structure of about 100 nm, the magnitude of the induced electric field is estimated to be 6×10^7 V m^{-1}. At this magnitude, no noticeable change in the line shape of the EL spectrum is detected for 30 min (Figures 4e and S5). It is worth noting that devices with ITO/ZnO/$CsPbCl_{1.5}Br_{1.5}$ NCs/TFB/MoO_3/Ag architecture operating under two times weaker electric field showed a pronounced redshift of EL peak from 485 to 518 nm for 10 min[15] (Figure 4e).

To vividly demonstrate a major improvement in the spectral stability, we present the comparative dynamics in the log−log scale in Figure 4f illustrating EL peak redshift of 0.7 nm only in our devices versus 33 nm value in the reference ones. Therefore, we claim our synthetic approach to be superior for the production of blue-emitting perovskite NCs resistant to electric field-induced ion segregation.

CONCLUSIONS

In summary, we have presented a novel approach for the preparation of $Cs(Pb_{0.88}Cd_{0.12})Br_3$ perovskite NCs. Our two-step synthesis includes the production of conventional $CsPbBr_3$ NCs and their doping with Cd^{2+} ions using reactive $Cd(OA)_2$ species in the presence of $[Br^-\cdots HOLAm^+]$ preventing the formation of structural defects at the NCs surface. The accurate values of the band gap energy for both materials in their bulk form have been predicted via DFT calculations. The resultant Cd-containing NCs with a mean size of 11 nm have been characterized using XRD, HRSTEM, and EDX methods confirming their crystal structure, high crystallinity, and even distribution of all the chemical elements

https://doi.org/10.1021/acsami.3c18122
ACS Appl. Mater. Interfaces 2024, 16, 11656−11664

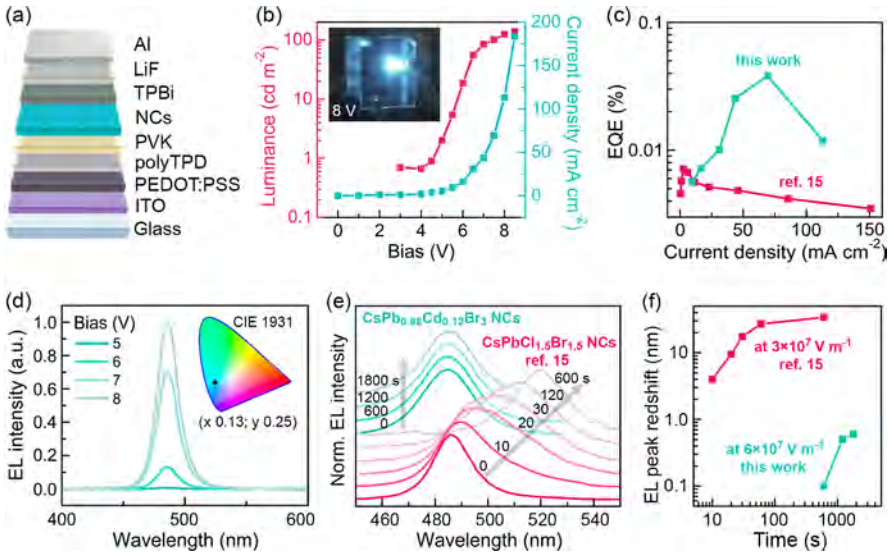

Figure 4. (a) Schematic illustration of the PeLED architecture. (b) Current density−voltage (J−V) and luminance−voltage (L−V) curves. Inset image demonstrates the PeLED operating at bias of 8 V. (c) EQE versus current density curves for blue-emitting PeLEDs based on $CsPb_{0.88}Cd_{0.12}Br_3$ (this work) and $CsPbCl_{1.5}Br_{1.5}$ NCs (redrawn with permission from ref 15, copyright © 2016, John Wiley and Sons). (d) EL spectra at various biases. Inserted plot is a CIE 1931 diagram describing the color of EL. (e) Evolution of normalized EL spectra of PeLEDs studied in this work and in ref 15 (redrawn with permission, copyright © 2016, John Wiley and Sons). One can see that Cd-doped NCs do not exhibit any noticeable redshift of the electroluminescence spectrum, whereas mixed-halide counterparts reveal rapid and dramatic redshift caused by the electric field-induced ion segregation phenomenon. (f) EL peak redshift versus time plot illustrating improved spectral stability of PeLEDs based on Cd-doped NCs operating under two times higher electric field than ones based on mixed-halide NCs reported in ref 15 (redrawn with permission, copyright © 2016, John Wiley and Sons).

in them as well as exact chemical composition. The colloidal NCs solution exhibited bright blue PL (λ_{max} = 485 nm) with PLQY = 89.9% and no change in the emission spectrum for 2 months. EL properties of the NCs have been studied on multilayer PeLEDs that revealed a turn-on bias of 4.5 V, maximum brightness of 137 cd m^{-2}, maximum EQE of 0.037%, and 0.7 nm spectral shift only at a magnitude of the electric field of 6×10^7 V m^{-1} for 30 min. The latter is a major improvement in EL spectral stability. We believe that our findings will expedite further progress in blue PeLEDs based on NCs resistant to electric field-induced ion segregation.

METHODS

Synthesis. All of the chemicals were purchased from Sigma-Aldrich and used as received unless otherwise noted.

Cs_2CO_3 (0.814 g, purity 99.9%), ODE (40 mL, purity 90%), and OA (2.5 mL, purity 90%) were loaded into a 100 mL flask, dried under vacuum at 120 °C for 1 h, and then heated up to 150 °C under stirring and N_2 protection, yielding a clear CsOA 0.125 M precursor solution. The solution was cooled down to room temperature for storage and preheated up to 120 °C before use.

$CdBr_2 \cdot [H_2O]_4$ (0.172 g, purity 99.9%), ODE (10 mL, purity 90%), OA (0.38 mL, purity 90%), and OLAM (0.39 mL, purity 90%) were loaded into a 50 mL flask, dried under vacuum at 120 °C for 1 h, and then heated up to 150 °C under stirring and N_2 protection, yielding a clear solution containing $Cd(OA)_2$ (0.5 mmol) and [Br$^-$···HOLAm$^+$] (1 mmol). The solution was cooled to room temperature for storage.

$PbBr_2$ (0.069 g, purity 99.99%) and ODE (5 mL) were loaded into a 50 mL 3-neck flask and dried under a vacuum for 1 h at 120 °C. OLAm (0.5 mL) and OA (0.5 mL) were injected at 120 °C under vacuum and stirred for 5 min. Then, the flask was filled with N_2 and heated up to 150 °C. After complete dissolution of the $PbBr_2$, the temperature was raised to 180 °C, and CsOA solution (0.4 mL) was quickly injected and, 10 s later, the reaction mixture was quenched using the ice bath.

To purify as-prepared $CsPbBr_3$ NCs, 15 mL of ODE was added to the product. After centrifuging at 5000 rpm for 5 min, a supernatant solution was discarded, and the sediment was redispersed in 15 mL of an ODE. $Cd(OA)_2$ precursor solution (0.320 g) was added to the latter one. Then, the mixture was poured into a two-neck flask, degassed under vacuum for 10 h at 80 °C and, afterward, stirred at 150 °C for 1 h to obtain $CsPb_{0.88}Cd_{0.12}Br_3$ NCs. The resultant solution was quenched using an ice bath, separated from byproducts by centrifuging at 5000 rpm for 5 min, and finally, redispersed in 10 mL of *n*-hexane.

DFT Modeling. The DFT calculations were performed by means of the GPAW software package.[42]

The initial configuration for an orthorhombic $CsPbBr_3$ cell with 20 atoms was adopted from Materials Project.[43] The $CsPb_{0.875}Cd_{0.125}Br_3$ structure was generated by $2 \times 2 \times 1$ translation of $CsPbBr_3$ unit cell resulting in 80 atoms cell and then two Pb atoms were randomly replaced by Cd.

The modified Broyden−Fletcher−Goldfarb−Shanno algorithm[44] was used to optimize the atom positions together with cell parameters for all cells generated. For geometry optimization, we used the modified for solids Perdew−Burke−Ernzerhof (PBEsol)[45] generalized gradient approximation exchange−correlation functional, Monkhrost-Pack (MP) grid with density 7 points/Å^{-1} was used in calculations, and the plane-wave basis with cutoff 700 eV. The force cutoff was set to 0.02 eV/Å.

Then, the GLLB-sc[46,47] exchange-correlation potential was used to correctly determine the band gap values. First, the electron density was calculated on a finer Γ-centered MP grid with a density of 15 points/Å^{-1} and then the band structure was unfolded with respect to the optimized $CsPbBr_3$ cell. Finally, the SOC was taken into account and calculated nonself-consistently in band structure calculations.

Structural and Optical Measurements. XRD pattern for NCs film was measured using a SmartLab diffractometer (Rigaku) equipped with a 9 kW rotating Cu anode X-ray tube. STEM images were obtained on a Titan Themis Z transmission electron microscope (Thermo Fisher Scientific). SEM images and EDX spectra were measured on an FEI Quanta Inspect S. The absorption spectrum of the colloidal solution was recorded on a UV-3600 spectrophotometer

https://doi.org/10.1021/acsami.3c18122
ACS Appl. Mater. Interfaces 2024, 16, 11656−11664

(Shimadzu). The PL spectrum of the colloidal solution and PLQY were measured on an RF-6000 spectrofluorometer (Shimadzu) equipped with an integrating sphere.

PeLEDs Fabrication and Characterization. To fabricate the ITO bottom electrode patterns, glass substrates coated with a solid ITO layer underwent laser lithography processing. For the deposition of hole transport layers, namely, Pedot/PSS, polyTPD, and PVK, along with an emitting layer of cadmium-doped perovskite NCs, a solution spin-coating technique was employed. The patterned glass substrates with ITO electrodes were subsequently subjected to a sequential ultrasonic treatment in deionized water, acetone, and isopropyl alcohol for 5 min each, followed by oxygen plasma treatment at 40 W for 5 min.

The application of the Pedot/PSS layer involved centrifuging the solution at 3000 rpm for 1 min, followed by annealing in air at 120 °C for 30 min. Similarly, solutions of polyTPD (8 mg per 1 mL toluene), PVK (5 mg per 1 mL chlorobenzene), and $CsPb_{0.88}Cd_{0.12}Br_3$ QDs in hexane were applied within a nitrogen glovebox using centrifugation speeds of 2000, 4000, and 1000 rpm, respectively. Subsequently, thermal annealing was performed at temperatures of 120, 140, and 100 °C, respectively.

To complete the device structure, an electron-transport TPBi layer (50 nm), a lithium fluoride layer (2 nm), and an aluminum electrode (100 nm) were deposited through a thermal vacuum sputtering.

The voltage-ampere and voltage-brightness characteristics of the fabricated devices were assessed by employing a comprehensive experimental setup. This setup comprised a Keithley 2400 current source and an Instrument Systems CAS 120 matrix spectroradiometer and was controlled utilizing the LabView software package.

■ ASSOCIATED CONTENT

Supporting Information

The Supporting Information is available free of charge at https://pubs.acs.org/doi/10.1021/acsami.3c18122.

FTIR spectrum of the stock solution, XRD pattern of $CsPbBr_3$ NCs, SEM images of a microscopic superlattice consisting of self-assembled $CsPb_{0.88}Cd_{0.12}Br_3$ NCs of 11 nm size, absorption and PL spectra of diluted $CsPbBr_3$ NCs colloidal solution, and electroluminescence dynamics of the PeLED operating at 6×10^7 V m^{-1} (PDF)

■ AUTHOR INFORMATION

Corresponding Authors

Yangyang Ju − *Beijing Key Laboratory of Nanophotonics and Ultrafine Optoelectronic Systems, Advanced Research Institute of Multidisciplinary Sciences, Beijing Institute of Technology, Beijing 100081, China*; Email: yangyangju@bit.edu.cn

Anatoly P. Pushkarev − *School of Physics and Engineering, ITMO University, St. Petersburg 197101, Russia*; orcid.org/0000-0002-1793-6812; Email: anatoly.pushkarev@metalab.ifmo.ru

Authors

Sergey S. Anoshkin − *School of Physics and Engineering, ITMO University, St. Petersburg 197101, Russia*

Elizaveta V. Sapozhnikova − *School of Physics and Engineering, ITMO University, St. Petersburg 197101, Russia*

Yibo Feng − *Beijing Key Laboratory of Nanophotonics and Ultrafine Optoelectronic Systems, School of Materials Science and Engineering, Beijing Institute of Technology, Beijing 100081, China*

Alexander Pavlov − *St. Petersburg Academic University, St. Petersburg 194021, Russia; Peter the Great St.Petersburg Polytechnic University, St.Petersburg 195251, Russia*; orcid.org/0000-0003-1125-6653

Roman G. Polozkov − *St. Petersburg Academic University, St. Petersburg 194021, Russia*

Alexey Yulin − *School of Physics and Engineering, ITMO University, St. Petersburg 197101, Russia*

Haizheng Zhong − *Beijing Key Laboratory of Nanophotonics and Ultrafine Optoelectronic Systems, School of Materials Science and Engineering, Beijing Institute of Technology, Beijing 100081, China*; orcid.org/0000-0002-2662-7472

Complete contact information is available at: https://pubs.acs.org/10.1021/acsami.3c18122

Author Contributions

#These authors contributed equally to this work.

Notes

The authors declare no competing financial interest.

■ ACKNOWLEDGMENTS

This work was supported by the Russian Science Foundation (project no. 23-72-00031) and by the Priority 2030 Federal Academic Leadership Program. The authors thank Prof. H.V. Demir for the fruitful discussion and Dr. V. Sheremet for SEM and EDX measurements. A.P. acknowledges the Ministry of Science and Higher Education of the Russian Federation (FSRM 2023-0007) for financial support and the Supercomputing Center of Peter the Great Saint-Petersburg Polytechnic University (SPbPU) for providing him with the opportunity to carry out large-scale simulations. STEM images and EDX maps were measured in the Advanced Imaging Core Facility (AICF) of the Skolkovo Institute of Science and Technology (Skoltech).

■ REFERENCES

(1) Dey, A.; Ye, J.; De, A.; Debroye, E.; Ha, S. K.; Bladt, E.; Kshirsagar, A. S.; Wang, Z.; Yin, J.; Wang, Y.; Quan, L. N.; Yan, F.; Gao, M.; Li, X.; Shamsi, J.; Debnath, T.; Cao, M.; Scheel, M. A.; Kumar, S.; Steele, J. A.; Gerhard, M.; Chouhan, L.; Xu, K.; Wu, X.-G.; Li, Y.; Zhang, Y.; Dutta, A.; Han, C.; Vincon, I.; Rogach, A. L.; Nag, A.; Samanta, A.; Korgel, B. A.; Shih, C.-J.; Gamelin, D. R.; Son, D. H.; Zeng, H.; Zhong, H.; Sun, H.; Demir, H. V.; Scheblykin, I. G.; Mora-Seró, I.; Stolarczyk, J. K.; Zhang, J. Z.; Feldmann, J.; Hofkens, J.; Luther, J. M.; Pérez-Prieto, J.; Li, L.; Manna, L.; Bodnarchuk, M. I.; Kovalenko, M. V.; Roeffaers, M. B. J.; Pradhan, N.; Mohammed, O. F.; Bakr, O. M.; Yang, P.; Müller-Buschbaum, P.; Kamat, P. V.; Bao, Q.; Zhang, Q.; Krahne, R.; Galian, R. E.; Stranks, S. D.; Bals, S.; Biju, V.; Tisdale, W. A.; Yan, Y.; Hoye, R. L. Z.; Polavarapu, L. State of The Art and Prospects for Halide Perovskite Nanocrystals. *ACS Nano* **2021**, *15*, 10775−10981.

(2) Brandt, R. E.; Stevanović, V.; Ginley, D. S.; Buonassisi, T. Identifying Defect-Tolerant Semiconductors with High Minority-Carrier Lifetimes: Beyond Hybrid Lead Halide Perovskites. *MRS Commun.* **2015**, *5*, 265−275.

(3) Pan, J.; Shang, Y.; Yin, J.; De Bastiani, M.; Peng, W.; Dursun, I.; Sinatra, L.; El-Zohry, A. M.; Hedhili, M. N.; Emwas, A.-H.; Mohammed, O. F.; Ning, Z.; Bakr, O. M. Bidentate Ligand-Passivated $CsPbI_3$ Perovskite Nanocrystals for Stable Near-Unity Photoluminescence Quantum Yield and Efficient Red Light-Emitting Diodes. *J. Am. Chem. Soc.* **2018**, *140*, 562−565.

(4) Zhang, B.; Goldoni, L.; Zito, J.; Dang, Z.; Almeida, G.; Zaccaria, F.; De Wit, J.; Infante, I.; De Trizio, L.; Manna, L. Alkyl Phosphonic Acids Deliver $CsPbBr_3$ Nanocrystals with High Photoluminescence Quantum Yield and Truncated Octahedron Shape. *Chem. Mater.* **2019**, *31*, 9140−9147.

(5) Imran, M.; Ijaz, P.; Goldoni, L.; Maggioni, D.; Petralanda, U.; Prato, M.; Almeida, G.; Infante, I.; Manna, L. Simultaneous Cationic and Anionic Ligand Exchange for Colloidally Stable $CsPbBr_3$ Nanocrystals. *ACS Energy Lett.* **2019**, *4*, 819−824.
(6) Grisorio, R.; Fasulo, F.; Muñoz-García, A. B.; Pavone, M.; Conelli, D.; Fanizza, E.; Striccoli, M.; Allegretta, I.; Terzano, R.; Margiotta, N.; Vivo, P.; Suranna, G. P. In Situ Formation of Zwitterionic Ligands: Changing the Passivation Paradigms of $CsPbBr_3$ Nanocrystals. *Nano Lett.* **2022**, *22*, 4437−4444.
(7) Protesescu, L.; Yakunin, S.; Bodnarchuk, M. I.; Krieg, F.; Caputo, R.; Hendon, C. H.; Yang, R. X.; Walsh, A.; Kovalenko, M. V. Nanocrystals of Cesium Lead Halide Perovskites ($CsPbX_3$, X= Cl, Br, and I): Novel Optoelectronic Materials Showing Bright Emission with Wide Color Gamut. *Nano Lett.* **2015**, *15*, 3692−3696.
(8) Maes, J.; Balcaen, L.; Drijvers, E.; Zhao, Q.; De Roo, J.; Vantomme, A.; Vanhaecke, F.; Geiregat, P.; Hens, Z. Light Absorption Coefficient of $CsPbBr_3$ Perovskite Nanocrystals. *J. Phys. Chem. Lett.* **2018**, *9*, 3093−3097.
(9) Herz, L. M. Charge-Carrier Mobilities in Metal Halide Perovskites: Fundamental Mechanisms and Limits. *ACS Energy Lett.* **2017**, *2*, 1539−1548.
(10) Zheng, W.; Wan, Q.; Liu, M.; Zhang, Q.; Zhang, C.; Yan, R.; Feng, X.; Kong, L.; Li, L. $CsPbBr_3$ Nanocrystal Light-Emitting Diodes with Efficiency up to 13.4% Achieved by Careful Surface Engineering and Device Engineering. *J. Phys. Chem. C* **2021**, *125*, 3110−3118.
(11) Tsai, H.; Shrestha, S.; Vilá, R. A.; Huang, W.; Liu, C.; Hou, C.-H.; Huang, H.-H.; Wen, X.; Li, M.; Wiederrecht, G.; Cui, Y.; Cotlet, M.; Zhang, X.; Ma, X.; Nie, W. Bright and Stable Light-Emitting Diodes Made with Perovskite Nanocrystals Stabilized in Metal−Organic Frameworks. *Nat. Photonics* **2021**, *15*, 843−849.
(12) Liu, M.; Wan, Q.; Wang, H.; Carulli, F.; Sun, X.; Zheng, W.; Kong, L.; Zhang, Q.; Zhang, C.; Zhang, Q.; Brovelli, S.; Li, L. Suppression of Temperature Quenching in Perovskite Nanocrystals for Efficient and Thermally Stable Light-Emitting Diodes. *Nat. Photonics* **2021**, *15*, 379−385.
(13) Shen, X.; Zhang, Y.; Kershaw, S. V.; Li, T.; Wang, C.; Zhang, X.; Wang, W.; Li, D.; Wang, Y.; Lu, M.; Zhang, L.; Sun, C.; Zhao, D.; Qin, G.; Bai, X.; Yu, W. W.; Rogach, A. L. Zn-Alloyed $CsPbI_3$ Nanocrystals for Highly Efficient Perovskite Light-Emitting Devices. *Nano Lett.* **2019**, *19*, 1552−1559.
(14) Guo, J.; Lu, M.; Zhang, X.; Sun, S.; Han, C.; Zhang, Y.; Yang, X.; Kershaw, S. V.; Zheng, W.; Rogach, A. L. Highly Stable and Efficient Light-Emitting Diodes Based on Orthorhombic γ-$CsPbI_3$ Nanocrystals. *ACS Nano* **2023**, *17*, 9290−9301.
(15) Li, G.; Rivarola, F. W. R.; Davis, N. J. L. K.; Bai, S.; Jellicoe, T. C.; de la Peña, F.; Hou, S.; Ducati, C.; Gao, F.; Friend, R. H.; Greenham, N. C.; Tan, Z.-K. Highly Efficient Perovskite Nanocrystal Light-Emitting Diodes Enabled by a Universal Crosslinking Method. *Adv. Mater.* **2016**, *28*, 3528−3534.
(16) Gangishetty, M. K.; Hou, S.; Quan, Q.; Congreve, D. N. Reducing Architecture Limitations for Efficient Blue Perovskite Light-Emitting Diodes. *Adv. Mater.* **2018**, *30*, 1706226.
(17) Hoke, E. T.; Slotcavage, D. J.; Dohner, E. R.; Bowring, A. R.; Karunadasa, H. I.; McGehee, M. D. Reversible Photo-Induced Trap Formation in Mixed-Halide Hybrid Perovskites for Photovoltaics. *Chem. Sci.* **2015**, *6*, 613−617.
(18) Yoon, S. J.; Kuno, M.; Kamat, P. V. Shift Happens. How Halide Ion Defects Influence Photoinduced Segregation in Mixed Halide Perovskites. *ACS Energy Lett.* **2017**, *2*, 1507−1514.
(19) Brennan, M. C.; Draguta, S.; Kamat, P. V.; Kuno, M. Light-Induced Anion Phase Segregation in Mixed Halide Perovskites. *ACS Energy Lett.* **2018**, *3*, 204−213.
(20) Bischak, C. G.; Hetherington, C. L.; Wu, H.; Aloni, S.; Ogletree, D. F.; Limmer, D. T.; Ginsberg, N. S. Origin of Reversible Photoinduced Phase Separation in Hybrid Perovskites. *Nano Lett.* **2017**, *17*, 1028−1033.
(21) Bischak, C. G.; Wong, A. B.; Lin, E.; Limmer, D. T.; Yang, P.; Ginsberg, N. S. Tunable Polaron Distortions Control the Extent of Halide Demixing in Lead Halide Perovskites. *J. Phys. Chem. Lett.* **2018**, *9*, 3998−4005.
(22) Barker, A. J.; Sadhanala, A.; Deschler, F.; Gandini, M.; Senanayak, S. P.; Pearce, P. M.; Mosconi, E.; Pearson, A. J.; Wu, Y.; Srimath Kandada, A. R.; Leijtens, T.; De Angelis, F.; Dutton, S. E.; Petrozza, A.; Friend, R. H. Defect-Assisted Photoinduced Halide Segregation in Mixed-Halide Perovskite Thin Films. *ACS Energy Lett.* **2017**, *2*, 1416−1424.
(23) Draguta, S.; Sharia, O.; Yoon, S. J.; Brennan, M. C.; Morozov, Y. V.; Manser, J. S.; Kamat, P. V.; Schneider, W. F.; Kuno, M. Rationalizing the Light-Induced Phase Separation of Mixed Halide Organic−Inorganic Perovskites. *Nat. Commun.* **2017**, *8*, 200.
(24) Liashenko, T. G.; Pushkarev, A. P.; Naujokaitis, A.; Pakštas, V.; Franckevičius, M.; Zakhidov, A. A.; Makarov, S. V. Suppression of Electric Field-Induced Segregation in Sky-Blue Perovskite Light-Emitting Electrochemical Cells. *Nanomaterials* **2020**, *10*, 1937.
(25) Imran, M.; Ramade, J.; Di Stasio, F.; De Franco, M.; Buha, J.; Van Aert, S.; Goldoni, L.; Lauciello, S.; Prato, M.; Infante, I.; Bals, S.; Manna, L. Alloy $CsCd_xPb_{1-x}Br_3$ Perovskite Nanocrystals: The Role of Surface Passivation in Preserving Composition and Blue Emission. *Chem. Mater.* **2020**, *32*, 10641−10652.
(26) Guo, J.; Fu, Y.; Lu, M.; Zhang, X.; Kershaw, S. V.; Zhang, J.; Luo, S.; Li, Y.; Yu, W. W.; Rogach, A. L.; Zhang, L.; Bai, X. Cd-Rich Alloyed $CsPb_{1-x}Cd_xBr_3$ Perovskite Nanorods with Tunable Blue Emission and Fermi Levels Fabricated Through Crystal Phase Engineering. *Adv. Sci.* **2020**, *7*, 2000930.
(27) Guo, J.; Hu, Q.; Lu, M.; Li, A.; Zhang, X.; Sheng, R.; Chen, P.; Zhang, Y.; Wu, J.; Fu, Y.; Sun, G.; Yu, W. W.; Bai, X. Pb^{2+} Doped $CsCdBr_3$ Perovskite Nanorods for Pure-Blue Light-Emitting Diodes. *Chem. Eng. J.* **2022**, *427*, 131010.
(28) Liu, J.; Song, K.; Shin, Y.; Liu, X.; Chen, J.; Yao, K. X.; Pan, J.; Yang, C.; Yin, J.; Xu, L.-J.; Yang, H.; El-Zohry, A. M.; Xin, B.; Mitra, S.; Hedhili, M. N.; Roqan, I. S.; Mohammed, O. F.; Han, Y.; Bakr, O. M. Light-Induced Self-Assembly of Cubic $CsPbBr_3$ Perovskite Nanocrystals Into Nanowires. *Chem. Mater.* **2019**, *31*, 6642−6649.
(29) Perdew, J. P.; Burke, K.; Ernzerhof, M. Generalized Gradient Approximation Made Simple. *Phys. Rev. Lett.* **1996**, *77*, 3865−3868.
(30) Zhao, X.; Tang, T.; Xie, Q.; Gao, L.; Lu, L.; Tang, Y. First-Principles Study on the Electronic and Optical Properties of the Orthorhombic $CsPbBr_3$ and $CsPbI_3$ with C_{mcm} Space Group. *New J. Chem.* **2021**, *45*, 15857−15862.
(31) Cohen, A. J.; Mori-Sánchez, P.; Yang, W. Fractional Charge Perspective on the Band Gap in Density-Functional Theory. *Phys. Rev. B* **2008**, *77*, 115123.
(32) Du, X.; He, D.; Mei, H.; Zhong, Y.; Cheng, N. Insights on Electronic Structures, Elastic Features and Optical Properties of Mixed-Valence Double Perovskites $Cs_2Au_2X_6$ (X= F, Cl, Br, I). *Phys. Lett. A* **2020**, *384*, 126169.
(33) Du, X.; He, D.; Liu, Y.; Cheng, N. Theoretical Investigations of Structural, Electronic, and Physical Properties of Rb_2BX_6 (B= Ti, Se, Pd; X= F, Cl, Br, I) Double Perovskites. *J. Appl. Phys.* **2020**, *128*, 235110.
(34) Even, J.; Pedesseau, L.; Jancu, J.-M.; Katan, C. Importance of Spin−Orbit Coupling in Hybrid Organic/Inorganic Perovskites for Photovoltaic Applications. *J. Phys. Chem. Lett.* **2013**, *4*, 2999−3005.
(35) Ma, X.-X.; Li, Z.-S. Influence of Sn/Ge Cation Exchange on Vacancy-Ordered Double Perovskite $Cs_2Sn_{1-x}Ge_xI_6$: A First-Principles Theoretical Study. *Phys. Status Solidi B* **2019**, *256*, 1800427.
(36) Paul, T.; Chatterjee, B.; Maiti, S.; Sarkar, S.; Besra, N.; Das, B.; Panigrahi, K.; Thakur, S.; Ghorai, U.; Chattopadhyay, K. Tunable Cathodoluminescence Over the Entire Visible Window from All-Inorganic Perovskite $CsPbX_3$ 1D Architecture. *J. Mater. Chem. C* **2018**, *6*, 3322−3333.
(37) Tao, S.; Schmidt, I.; Brocks, G.; Jiang, J.; Tranca, I.; Meerholz, K.; Olthof, S. Absolute Energy Level Positions in Tin-and Lead-Based Halide Perovskites. *Nat. Commun.* **2019**, *10*, 2560.
(38) Rodová, M.; Brožek, J.; Knížek, K.; Nitsch, K. Phase Transitions in Ternary Caesium Lead Bromide. *J. Therm. Anal. Calorim.* **2003**, *71*, 667−673.

https://doi.org/10.1021/acsami.3c18122
ACS Appl. Mater. Interfaces 2024, 16, 11656−11664

(39) Brennan, M. C.; Toso, S.; Pavlovetc, I. M.; Zhukovskyi, M.; Marras, S.; Kuno, M.; Manna, L.; Baranov, D. Superlattices Are Greener on the Other Side: How Light Transforms Self-Assembled Mixed Halide Perovskite Nanocrystals. *ACS Energy Lett.* **2020**, *5*, 1465−1473.
(40) Vashishtha, P.; Ng, M.; Shivarudraiah, S. B.; Halpert, J. E. High Efficiency Blue and Green Light-Emitting Diodes Using Ruddlesden−Popper Inorganic Mixed Halide Perovskites with Butylammonium Interlayers. *Chem. Mater.* **2019**, *31*, 83−89.
(41) Gets, D.; Alahbakhshi, M.; Mishra, A.; Haroldson, R.; Papadimitratos, A.; Ishteev, A.; Saranin, D.; Anoshkin, S.; Pushkarev, A.; Danilovskiy, E.; Makarov, S.; Slinker, J. D.; Zakhidov, A. A. Reconfigurable Perovskite LEC: Effects of Ionic Additives and Dual Function Devices. *Adv. Opt. Mater.* **2021**, *9*, 2001715.
(42) Enkovaara, J.; Rostgaard, C.; Mortensen, J. J.; Chen, J.; Dułak, M.; Ferrighi, L.; Gavnholt, J.; Glinsvad, C.; Haikola, V.; Hansen, H. A.; Kristoffersen, H. H.; Kuisma, M.; Larsen, A. H.; Lehtovaara, L.; Ljungberg, M.; Lopez-Acevedo, O.; Moses, P. G.; Ojanen, J.; Olsen, T.; Petzold, V.; Romero, N. A.; Stausholm-Møller, J.; Strange, M.; Tritsaris, G. A.; Vanin, M.; Walter, M.; Hammer, B.; Häkkinen, H.; Madsen, G. K. H.; Nieminen, R. M.; Nørskov, J. K.; Puska, M.; Rantala, T. T.; Schiøtz, J.; Thygesen, K. S.; Jacobsen, K. W. Electronic Structure Calculations with GPAW: a Real-Space Implementation of the Projector Augmented-Wave Method. *J. Phys.: Condens. Matter* **2010**, *22*, 253202.
(43) Jain, A.; Ong, S. P.; Hautier, G.; Chen, W.; Richards, W. D.; Dacek, S.; Cholia, S.; Gunter, D.; Skinner, D.; Ceder, G.; Persson, K. A. Commentary: The Materials Project: A Materials Genome Approach to Accelerating Materials Innovation. *APL Mater.* **2013**, *1*, 011002.
(44) Nocedal, J.; Wright, S. J. *Numerical Optimization*; Springer Science & Business Media, 2006.
(45) Perdew, J. P.; Ruzsinszky, A.; Csonka, G. I.; Vydrov, O. A.; Scuseria, G. E.; Constantin, L. A.; Zhou, X.; Burke, K. Restoring the Density-Gradient Expansion for Exchange in Solids and Surfaces. *Phys. Rev. Lett.* **2008**, *100*, 136406.
(46) Kuisma, M.; Ojanen, J.; Enkovaara, J.; Rantala, T. T. Kohn-Sham Potential with Discontinuity for Band Gap Materials. *Phys. Rev. B* **2010**, *82*, 115106.
(47) Castelli, I. E.; Olsen, T.; Datta, S.; Landis, D. D.; Dahl, S.; Thygesen, K. S.; Jacobsen, K. W. Computational Screening of Perovskite Metal Oxides for Optimal Solar Light Capture. *Energy Environ. Sci.* **2012**, *5*, 5814−5819.

https://doi.org/10.1021/acsami.3c18122
ACS Appl. Mater. Interfaces 2024, 16, 11656−11664